HHS Public Access

Author manuscript

Ophthalmology. Author manuscript; available in PMC 2016 December 01.

Published in final edited form as:

Ophthalmology. 2015 December ; 122(12): 2532–2544. doi:10.1016/j.ophtha.2015.08.029.

Ultrahigh Speed Swept Source OCT Angiography in Non-Exudative Age-Related Macular Degeneration with Geographic Atrophy

WooJhon Choi, PhD[1,*], **Eric M. Moult, BS**[1,2,*], **Nadia K. Waheed, MD**[3], **Mehreen Adhi, MD**[3], **ByungKun Lee, MS**[1], **Chen D. Lu, MS**[1], **Talisa De Carlo, BS**[3], **Vijaysekhar Jayaraman, PhD**[4], **Philip J. Rosenfeld, MD, PhD**[5], **Jay S. Duker, MD**[3], and **James G. Fujimoto, PhD**[1]

[1]Massachusetts Institute of Technology, Department of Electrical Engineering and Computer Science, and Research Laboratory of Electronics, Cambridge, MA

[2]Harvard-MIT Division of Health Sciences and Technology, Cambridge, MA

[3]Tufts University Medical Center, New England Eye Center, Boston, MA

[4]Praevium Research Inc., Santa Barbara, CA

[5]University of Miami Miller School of Medicine, Bascom Palmer Eye Institute, Department of Ophthalmology, Miami, FL

Abstract

PURPOSE—To investigate ultrahigh speed, swept source optical coherence tomography (SSOCT) angiography for visualizing vascular changes in eyes with non-exudative age-related macular degeneration (AMD) with geographic atrophy (GA).

DESIGN—Observational, prospective, cross-sectional study.

PARTICIPANTS—A total of 63 eyes from 32 normal subjects and 12 eyes from 7 patients with non-exudative AMD with GA.

METHODS—A 1050 nm, 400 kHz A-scan rate SSOCT system was used to perform volumetric optical coherence tomography angiography (OCTA) of the retinal and choriocapillaris (CC) vasculatures in normal subjects and patients with non-exudative AMD with GA. OCTA using

Corresponding Author/Reprint Requests: Correspondence to James G. Fujimoto, PhD, Department of Electrical Engineering and Computer Science, and Research Laboratory of Electronics, Massachusetts Institute of Technology, 77 Massachusetts Avenue, 36-345, Cambridge, MA 02139. jgfuji@mit.edu.

*These two authors contributed equally.

Meeting Presentation

Results presented in part at: Association for Research in Vision and Ophthalmology meeting, May 2014, Orlando, Florida.

Financial Disclosure

The authors have made the following financial disclosures: JSD: consultant and research support from Carl Zeiss Meditec Inc. and Optovue Inc. JGF: royalties from intellectual property owned by Massachusetts Institute of Technology and licensed to Carl Zeiss Meditec Inc. and Optovue Inc., and stock options with Optovue Inc. PJR: research support from Carl Zeiss Meditec Inc.

variable interscan time analysis (VISTA) was performed to assess CC alteration and differentiate varying degrees of CC flow impairment.

MAIN OUTCOME MEASURES—Qualitative comparison of retinal and CC vasculatures in normal subjects versus those in patients with a clinical diagnosis of non-exudative AMD with GA.

RESULTS—In all 12 eyes with GA, OCTA showed pronounced CC flow impairment within the region of GA. In 10 of the 12 eyes with GA, OCTA with VISTA showed milder CC flow impairment extending beyond the margin of GA. Of the 5 eyes exhibiting foveal sparing GA, OCTA showed CC flow within the region of foveal sparing in 4 of the eyes.

CONCLUSIONS—The ability of ultrahigh speed, swept source OCTA to visualize alterations in the retinal and CC vasculatures noninvasively makes it a promising tool for assessing non-exudative AMD with GA. OCTA using VISTA can distinguish varying degrees of CC alteration and flow impairment and may be useful for elucidating disease pathogenesis, progression, and response to therapy.

Introduction

Age-related macular degeneration (AMD) is a leading cause of vision loss and impairment in developed countries. Historically, the most severe vision loss has been associated with the exudative form of AMD (wet AMD), which is characterized by choroidal neovascularization (CNV). However, with the success of vascular endothelial growth factor (VEGF) inhibitors, the advanced non-exudative form of the disease (dry AMD), which is characterized by geographic atrophy (GA), is likely to become the leading cause of severe vision loss in the future. Optical coherence tomography (OCT) is a valuable tool for imaging the structural changes associated with AMD progression, as well as for monitoring treatment response. Until recently, however, OCT has been unable to visualize the pathological vascular changes associated with non-exudative AMD with GA. Instead, vascular changes in the retina and choroid have been visualized using fluorescein angiography (FA) and indocyanine green angiography (ICGA). However, these modalities have inherent disadvantages for visualizing the choriocapillaris (CC) and choroid and have had limited utility in assessing non-exudative AMD with GA.

Multiple histopathological studies have investigated the role of the choroid in non-exudative AMD with GA. The choroid, the highly vascular tissue responsible for nourishing the outer retinal layers, is comprised of five layers, three of which are vascular: the CC, Sattler's layer, and Haller's layer. The CC, the thin capillary layer of the choroid, is located adjacent to Bruch's membrane and has a mutualistic relationship with the retinal pigment epithelium (RPE).[1–4] The hallmark of advanced non-exudative AMD is the formation of geographic atrophy (GA), which is characterized by the loss of photoreceptors, RPE, and CC.[1, 2] The primary site of injury responsible for GA is currently unknown and a topic of debate.[2–7]

The absence of an imaging modality capable of providing adequate visualization of the CC has hindered the understanding of GA. In particular, while FA enables visualization of the retinal vasculature, it is challenging to use FA to image the CC and choroid for two reasons. First, the blue-green excitation wavelength of fluorescein is partially absorbed by the macular xanthophyll and RPE. Second, because ~20% of the injected fluorescein does not

bind to albumin, there is leakage from the CC fenestrations, which creates early, diffuse hyperfluorescence and obscures the vasculature.[8] In contrast, the near infrared excitation wavelength and high bonding affinity of ICGA enables visualization of choroidal circulation.[8] ICGA has also been demonstrated for visualization of the CC circulation.[9] However, since ICGA is not depth resolved, separating CC blood flow from that of deeper choroidal vasculature is a complex task and, for this reason, ICGA has not gained widespread acceptance for CC visualization.[9, 10]

OCT angiography (OCTA) is a relatively new imaging technique that generates three-dimensional images of vasculature *in vivo* and without dye injection.[11–19] Unlike dye-based angiography methods, such as FA and ICGA, OCTA is noninvasive and fast, having a typical acquisition time of under 4 seconds. OCTA involves acquiring repeated B-scans, in rapid succession, from the same retinal location. The principle of OCTA is that repeated imaging of stationary tissue yields a series of identical B-scans. However, if there is motion from blood flow, then the repeated B-scans will change over time, and this change can be quantified and displayed.

OCTA requires different acquisition protocols, different processing techniques, and ultimately measures different quantities than traditional, structural, OCT; consequentially, an alternate terminology is needed (Table 1). Briefly summarizing, a pixel-by-pixel *decorrelation signal* is computed from repeated B-scans acquired at the same retinal location; volumetric decorrelation data are generated by acquiring multiple sets of repeated B-scans, with each set from a different retinal location. An OCTA image is generated by displaying the decorrelation signal as a grayscale image. In this manuscript, we use the convention of associating lighter shaded pixels with larger decorrelations and darker shaded pixels with smaller decorrelations. Faster blood flows produce larger decorrelation signals and therefore appear lighter than slower blood flows.

It is important to note that the dynamic range of OCTA is limited and that there is a *slowest detectable flow* and a *fastest distinguishable flow*. Flows slower than the slowest detectable flow produce decorrelations that are indistinguishable from background noise and are therefore undetectable. These flows are below the sensitivity threshold. Flows faster than the fastest distinguishable flow all produce similar decorrelation signals and therefore are indistinguishable from one another. These flows are above the saturation limit. The time between the repeated B-scans, the *interscan time*, is a critical parameter that governs how the decorrelation signal relates to the physical erythrocyte flow speeds. Increasing the interscan time allows the erythrocytes to move a greater distance between successive B-scans and therefore increases the decorrelation signal. Increasing the interscan time reduces both the slowest detectable flow and the fastest distinguishable flow. In practice, increasing the interscan time also increases the noise, because there is increased sensitivity to parasitic eye motion.

Since the retinal and CC vasculatures are predominantly oriented along *en face* planes, OCTA requires dense volumetric scanning of the retina. This requirement, combined with the need for repeated B-scan acquisition, makes high imaging speeds necessary for OCTA; this has created a gap between the technological development and clinical application of

OCTA. Recently OCTA has been applied in small numbers of patients with non-exudative AMD: in 2013 Kim et al performed OCTA in 1 non-exudative AMD patient with GA,[20] and in 2014 Schwartz et al performed OCTA in 1 non-exudative AMD patient.[21] Both studies were performed at OCT A-scan rates of ~100 kHz or less, making the clinical application of the technology challenging due to the small fields of view and limited image quality. Commercial OCTA instruments recently became available outside of the United States with the introduction of the 70 kHz Avanti RTVue XR equipped with the AngioVue software (Optovue, Inc., Fremont, CA). While the hardware system is available in the United States, software approval is pending. Additionally, there are multiple companies developing instruments with OCTA capabilities, suggesting that OCTA will likely play an increasing role in the clinical setting.

The recent development of swept light sources has enabled a dramatic increase in ophthalmic OCT imaging speeds. Our group recently demonstrated ophthalmic swept-source OCT (SSOCT) using a vertical cavity surface emitting laser (VCSEL)[22] and later developed a phase stable ultrahigh speed SSOCT prototype with a 400 kHz A-scan rate.[23] This instrument is ~4–10 times faster than standard commercial ophthalmic OCT systems.

The purpose of this study is to assess ultrahigh speed swept source OCTA and variable interscan time analysis (VISTA) as a modality with which to visualize vascular changes that occur in the retina and CC of patients with non-exudative AMD with GA.

Methods

This study was approved by the Institutional Review Boards at the Massachusetts Institute of Technology (MIT) and Tufts Medical Center. All participants were imaged in the ophthalmology clinic at the New England Eye Center (NEEC) at Tufts Medical Center. Written informed consent was obtained from all subjects prior to imaging. The research adhered to the Declaration of Helsinki and the Health Insurance Portability and Accountability Act. All subjects underwent a complete ophthalmic examination including a detailed history, refraction, intraocular pressure measurement, anterior segment examination, and a dilated fundus examination by a general ophthalmologist or a retinal specialist at NEEC. Select patients received color fundus photography, fundus autofluorescence (FAF), FA, and ICGA, as clinically indicated. Normal subjects were defined as having no abnormalities on ophthalmic examination except for an age appropriate cataract, normal ophthalmic fundus examinations, normal visual fields, refraction less than or equal to 6D, and no history of diabetes.

OCTA was performed using an ultrahigh speed SSOCT research prototype developed at MIT and deployed to NEEC in November, 2013. A similar OCT system was described in detail previously[23] and therefore only key characteristics are summarized herein. The prototype technology used a VCSEL swept light source with a 400 kHz A-scan rate. The light source was centered at 1050 nm which, when compared to the 840 nm wavelengths used in most commercial system, enables deeper light penetration into the RPE and choroid, as well as improved immunity to ocular opacities.[24] OCT interferometric signals were acquired with an analog-to-digital acquisition card externally clocked at a maximum

frequency of ~1.1 GHz using an external Mach-Zehnder interferometer. A fiber Bragg grating was used to stabilize the interferometric signal, resulting in a phase stability of ~1.5 mrad at a signal-to-noise ratio of 57 dB. The imaging range was ~2.1 mm in tissue and the axial and transverse resolutions in tissue were ~8–9 μm and ~15 μm full-width at half-maximum (FWHM), respectively. The measured sensitivity was ~98 dB using ~1.8 mW incident power.

We performed OCTA with 6 mm × 6 mm and 3 mm × 3 mm fields of view. For both fields of view, 5 repeated B-scans from 500 uniformly spaced locations were sequentially acquired. Each B-scan consisted of 500 A-scans and the interscan time was ~1.5 ms (accounting for the galvanometer mirror scanning duty cycle). A total of 5 × 500 × 500 A-scans were acquired per OCTA volume with an acquisition time of ~3.8 s. OCTA images were generated by calculating the decorrelation signal on a pixel-by-pixel basis between sequential OCT B-scans (1↔2, 2↔3, 3↔4, 4↔5) acquired from the same location with a ~1.5 ms interscan time. To compensate for eye motion artifacts, which would produce decorrelation noise, repeated B-scans were motion corrected using a rigid registration algorithm.[25] For each location, we averaged the 4 resulting decorrelation images to improve the OCTA signal-to-noise ratio. This operation was performed at all B-scan locations in order to obtain a three-dimensional OCTA decorrelation signal.

The decorrelation signal in OCTA must be interpreted with care. In particular, a low decorrelation signal may be due to the complete absence of flow and vasculature. This condition is termed *atrophy*. Alternatively, a low decorrelation signal may also be due to slow blood flow but intact vasculature, a condition termed *flow impairment*. Collectively, atrophy and flow impairment are different types of *CC alteration* (Table 2 lists terminology for describing *en face* OCTA of the CC).

It is possible to differentiate varying degrees of flow impairment by varying the interscan time. This method, variable interscan time analysis (VISTA), is shown in Figure 1. VISTA is conceptually similar to previously proposed techniques, such as multi-timescale SSADA (MSSADA) by Tokayer et al,[26] and dual-beam Doppler microangiography by Makita et al.[27] VISTA scales the slowest detectable flow and fastest distinguishable flow to overcome dynamic range limitations. In particular, analyzing pairs of B-scans that have longer interscan times reduces the slowest detectable flow, improving sensitivity (Figure 1). In practice, the increase in interscan time, and corresponding sensitivity improvement, is limited by the ability to compensate parasitic eye motion. In addition to improving sensitivity, analyzing B-scans that have longer interscan times also reduces the fastest distinguishable flow, making saturation occur more easily and limiting the ability to differentiate flows. The converse is also true: analyzing B-scans that have a shorter interscan time reduces sensitivity, but improves differentiation of different flows by increasing the fastest distinguishable flow and reducing saturation effects (Figure 1).

VISTA can be performed using a single scanning protocol with three or more repeated B-scans, calculating the OCTA decorrelation between pairs of B-scans with different interscan times. In our study, we used two different interscan times, a ~3.0 ms interscan time by correlating every second B-scan (1↔3, 2↔4, 3↔5) and ~1.5 ms interscan time by

correlating sequential B-scans (1↔2, 2↔3, 3↔4, 4↔5). Since our acquisition protocol acquired 5 repeated B-scans per location, VISTA could be performed using a single data acquisition and multiple decorrelations from image pairs could be averaged to increase signal-to-noise.

In this study, volumetric OCTA data were generated containing the retinal, choroidal, and CC vasculatures. In order to separately visualize the retinal and CC vasculatures, both Bruch's membrane and the internal limiting membrane (ILM) were semi-automatically segmented using OCT B-scans. Exploiting the co-registration property of the OCT and OCTA data allows the segmentation contours from the structural OCT volume to be applied to the OCTA volume directly. *En face* retinal OCTA images were created by maximum projection between the ILM and Bruch's membrane. When generating an *en face* OCTA image of the CC it would be ideal if a slab immediately below the Bruch's membrane that exactly corresponds to the CC could be selected. Unfortunately, because the CC is a thin monolayer network of capillaries (~6.5 μm–10 μm axial diameter in the normal macula[28, 29]) such a precise selection requires segmentation with pixel, or sub-pixel, accuracy and therefore would be prone to errors. Mistakenly visualizing a depth anterior to the CC can result in artifacts because there is no flow in Bruch's membrane or RPE.

As discussed in Moult et al,[30] the CC can be more reliably visualized by selecting a slab slightly posterior to the CC. Such visualization is possible because the CC flow produces OCTA decorrelation signals that are persistent at depths posterior to the anatomical CC. This depth persistence phenomenon has been variably termed *decorrelation tails* (because vasculature generates "tail"-like features on cross-sectional OCTA images), *OCTA shadowing*, and *OCTA projection* (because vasculature at superficial levels produces the appearance of flow at deeper levels). The phenomenon occurs because erythrocytes are highly scattering and produce fluctuations in the OCT beam below them as they flow, causing deeper structures to exhibit variations in the OCT signal with time. Although this can produce artifacts, such as the appearance of retinal vasculature at the level of the RPE, it also enables more robust visualization of vasculature.

In order to visualize the CC, we selected the first *en face* plane below the Bruch's membrane that was not affected by segmentation errors. In this paper we use the term *CC slab* to refer to a slab of the OCTA volume that lies below the actual CC, but that reflects the CC patterning, and therefore CC flow. In this study our CC slab thickness was 4.4 μm, which was set by the configuration and calibration of our SSOCT instrument. It should be noted that since our CC slab thickness is less than the optical FWHM axial resolution, a given slab should be interpreted as containing an average of the structures within the FWHM axial resolution. The ability to visualize the CC using this method is illustrated in Figure 2, in which *en face* intensity-based structural OCT images are paired with *en face* OCTA images. The CC, which cannot be seen in *en face* structural OCT, corresponds to the depths spanned by the slabs of Figures 2C and 2D. Note that the CC patterning exhibited in Figure 2 is consistent with the known structure of the CC from scanning electron microscopy studies,[31] as noted by Choi et al[32] and supports the assertion that OCTA visualizes the CC. It is also important to note that the CC patterning seen in Figures 2C and 2D is persistent in depth through to Figure 2J, which allows the CC slabs to be examined by using slabs of the OCTA

volume that lie below the CC. This reduces the sensitivity of the *en face* OCTA image to small segmentation errors, improving the potential clinical utility.

Results

A total of 32 normal subjects and 7 patients with non-exudative AMD with GA were included in this study (Table 3).

Normal subjects

The group of normal subjects (63 eyes from 32 subjects) recruited for the study had a mean age (± std.) of 40.7 ± 14.1 years (range 19 to 70 years). Among the 63 eyes imaged, 33 eyes were from subjects 40 years or older and 7 were from subjects 60 years or older. Figure 3 shows representative OCTA images of the retinal and CC vasculatures from a subset of the normal subjects. While the 6 mm × 6 mm field of view provides wider retinal coverage, the 3 mm × 3 mm field of view has superior image quality because of its higher sampling density. In this study, we qualitatively assessed the vessel ratio (Table 2) but did not evaluate it quantitatively. While variation in the vessel ratio among normal subjects was observed, the CC in the macular region of normal subjects was uniformly dense and homogeneous. Although the number of normal subjects older than 60 was limited, a clear age dependency in the CC vessel ratio among this cohort was not qualitatively observed; however, a general trend of reduced choroidal thickness among older normal subjects was observed, which has been documented previously.[33]

Patients with non-exudative AMD with GA

The group of patients with non-exudative AMD and GA (12 eyes from 7 subjects) had a mean age (± std.) of 75.9 ± 6.1 years (range 65 to 82 years). Figure 4 shows FAF, OCT, and OCTA with VISTA of a representative 75-year-old patient with non-exudative AMD with GA. Figure 4B, which is the mean projection of the entire OCT volume, shows the region of GA, outlined by the yellow dashed contour, which agrees well with region of GA shown in the FAF. Figure 4C shows the mean *en face* projection of the OCTA volume through the depths spanned by the retinal vasculature, which appears normal. Figure 4D shows a 4.4 μm thick *en face* OCTA CC slab corresponding to a ~1.5 ms interscan time; Figure 4E shows the same 4.4 μm thick CC slab as in Figure 4D, but from an OCTA volume corresponding to a ~3.0 ms effective interscan time. The yellow dashed contour of Figure 4B is superimposed on Figures 5D and 5E for reference. Areas with low decorrelation signal are notable outside the GA margin and are particularly evident in Figure 4D. Figures 5F and 5G provide enlarged views of the solid orange and green boxes of Figures 5D and 5E, respectively. Note how there is vasculature that is visible in Figure 4G but not visible in Figure 4F. This illustrates the capability of VISTA to shift the range of the detectable flow speeds. Figures 4H and 4I show enlarged views of the dashed orange and green boxes that straddle the GA boundary in Figures 4D and 4E, respectively. Note that some of the areas with low decorrelation signal in Figure 4H have increased decorrelation signal in Figure 4I. Although care must be taken to avoid interpreting motion artifacts as blood flow, as addressed in the Discussion section of this paper, we believe that the additional decorrelation signal of 4I corresponds to blood flow, not noise. Additional evidence supporting this belief is provided

in Figure 4H and 5I where we see that increasing the interscan time increases the decorrelation of vessels significantly more than it increases the background noise level. OCT and OCTA B-scans through the red, blue, and purple horizontal dashed lines in Figure 4D are shown in Figures 4J–4L, respectively. It should be emphasized that Figures 4B–4L were generated from a single volumetric data set and are therefore intrinsically co-registered. Finally note that this eye exhibits foveal sparing, which appears as a dark island at the fovea in the *en face* OCT image (white arrow of Figure 4B); CC flow corresponding to the foveal sparing is also apparent in the *en face* OCTA CC slab (white arrow of Figure 4D). Of the 12 eyes with GA, 5 eyes had foveal sparing; OCTA showed CC flow at the fovea in 4 of these eyes.

Additional representative OCT and OCTA images from patients with non-exudative AMD with GA are shown in Figure 5. CC alterations extending beyond the GA margin were clearly present in 10 of the 12 eyes with GA. The remaining two eyes that did not show CC alterations beyond the region of GA were from the same patient. One of these two eyes is shown in Figure 5D.

Finally, in 2 of the 12 eyes with GA, using OCTA, previously undiagnosed choroidal neovascularization (CNV) was seen. Neither of these two eyes had significant subretinal fluid visible on OCT, nor was there evidence of exudation on the fundus photograph; as such, concurrent FA was not performed. Although it was not explicitly confirmed that these eyes had CNV on FA, OCTA clearly shows abnormal vasculature above the Bruch's membrane in both *en face* and cross-sectional images. In both of the cases the CNV was located above surviving RPE cells. One of these eyes is shown in Figure 6.

Discussion

An important finding of this study is that OCTA revealed CC alterations beyond the GA margin in 10 of the 12 eyes with GA. Using VISTA we showed that in all 10 of these eyes CC flow impairment outside the regions of GA was less pronounced than flow impairment occurring within the GA regions. These observations are interesting because of the mutualistic relationship of the CC and RPE, which has generated debate as to whether it is the CC or the RPE that is the primary site of injury in GA. This debate has led to the CC-RPE interaction in AMD being carefully investigated in several studies.[2–7]

In a series of histological studies McLeod et al have observed that CC loss was linearly related to RPE loss in regions of GA and that there was a 50% loss of CC density in regions of complete RPE atrophy; in no regions was a complete atrophy of CC observed.[2, 7] Based on these observations they concluded that the primary insult in GA appeared to be at the RPE. A recent study by Biesemeier et al, which used a combination of light and electron microscopy, suggested that CC breakdown precedes retinal degeneration in AMD.[5]

Due to the differences between OCT and histology, caution should be exercised when comparing observations derived from the two techniques. First, OCTA is an *in vivo* technique that images flow as a surrogate for CC function while histopathology studies are performed on excised samples and examine the static structure of the CC. However, lectin[34]

and alkaline phosphatase[35] histochemistry, as well as examination of the endothelial ultrastructure with electron microscopy,[5] have been used to determine vessel viability, allowing histopathology studies to make statements about CC flow as well as CC structure. Second, compared to histology, it is difficult to distinguish flow impairment from atrophy using OCTA. This difficulty, due to OCTA having a slowest detectable flow limited by parasitic eye motion, is a particular concern in regions of GA, where vessel constriction, and hence reduced flow speeds, is observed.[2, 5] Consequentially, although we observed that most GA regions exhibited no detectable decorrelation signal, we cannot conclude whether this was a consequence of atrophy or pronounced flow impairment. Based on the preponderance of histopathology evidence,[1, 2, 5, 7, 28] however, we suspect that the absence of detectable flow on OCTA is attributable to a combination of both.

Using the VISTA algorithm we demonstrated that there was CC flow impairment beyond the GA margins and that, when such flow impairment was present, it was less pronounced than the flow impairment within GA margins—increasing the interscan time showed increases in decorrelation signal around the margins of GA, but not within the regions of GA. This observation is consistent with findings reported in histology.[2, 5] Furthermore, while CC flow impairment outside the GA margin was present in 10 of the 12 eyes with GA, 2 of the 12 eyes, both of which were from the same patient, exhibited minimal CC flow impairment beyond the GA margin (one such eye is shown in Figure 5D). These two patterns of CC alteration (CC alteration both inside and outside the GA margin, versus CC alteration only inside the region of GA) may be related to the two patterns of photoreceptor disruption (photoreceptor disruption both inside and outside the GA margin, versus photoreceptor disruption only inside the GA margin) that have been observed in both histology and high resolution OCT/combined OCT and scanning laser ophthalmoscope (SLO) studies.[36–38] Future studies combining OCTA with ultrahigh resolution OCT imaging would help elucidate the relationship between CC flow impairment and photoreceptor disruption at the margins of GA.

In 2 of the 12 eyes with GA, previously undiagnosed and clinically silent CNV was detected using OCTA. This result is consistent with those of Bhutto et al and Sunness et al, who reported finding CNV in some eyes with GA.[4, 39] Consistent with their findings, in the 2 eyes in which we detected CNV, the lesion existed over surviving RPE cells. It has been hypothesized that CNV is associated with surviving RPE because the RPE cells provide the stimulus for the formation or stabilization of new blood vessels.[4]

OCTA offers several advantages over conventional dye-based angiography techniques. First and foremost, FA or ICGA is rarely justified in the setting of non-exudative AMD, while OCTA is completely safe and noninvasive. Moreover, unlike dye-based angiography, which is time consuming and has a limited time window for imaging after injection, OCTA is fast, can be performed at any time and, potentially, during every patient visit. OCTA also enables depth resolved imaging of the retinal, CC, and choroidal vasculatures. Furthermore, since both structural and vascular information are derived from the same acquisition, the data are intrinsically co-registered. This co-registration property makes volumetric OCTA a powerful tool for comprehensive assessment of retinal disease.

An important advantage of ultrahigh speed OCT technology is the ability to acquire high quality OCTA images over wide fields of view. In this study, high pixel density *en face* OCTA images over wide, 6 mm × 6 mm, field sizes were achievable because of the 400 kHz A-scan rate prototype technology. In comparison, an instrument operating at a 100 kHz A-scan rate would be limited to a 4× smaller field of view should a similar quality OCTA image be desired. Wide fields of view are important because the region of interest in patients with GA is often larger than 3 mm × 3 mm. Fast imaging speeds also enable the acquisition of more repeated B-scans from the same location, which allows VISTA to be performed and varying degrees of CC flow impairment to be differentiated.

OCTA data must be interpreted with care and special attention should be paid to the distinction between atrophy and flow impairment. In particular, although increasing the interscan time increases the sensitivity of OCTA to slow flows, it also increases noise from eye motion artifacts. The effect of noise on the visualization of larger vessels is less severe (Figure 4F and Figure 4G) because these vessels have fast flows and large *en face* dimensions. Visualization of the CC is, however, more affected by noise (Figure 4H and Figure 4I) and distinguishing CC flow versus eye motion artifacts can be challenging if the noise is increased. The deleterious effects of eye motion limited VISTA's ability to differentiate between CC flow impairment and CC atrophy definitively. Despite this limitation, we believe that VISTA is a useful method for OCTA studies because it can increase the dynamic range of OCTA and distinguish degrees of flow impairment, which would not be detectable using a fixed interscan time. Furthermore, improved image registration and OCTA processing algorithms promise to better suppress eye motion artifacts, enabling longer interscan times with reduced parasitic eye motion noise, thereby improving sensitivity to very slow flows.

In addition to the limited sensitivity to slow flows, potential artifacts from signal attenuation also need to be considered when interpreting OCTA data. OCTA processing involves a thresholding step that is performed prior to calculating decorrelations in order to prevent noise from generating false flow. This thresholding means that areas having flow but low signal may not have a decorrelation signal and may therefore appear as having no flow on OCTA. Stated another way, OCTA can only be obtained from structures that have a sufficient structural OCT signal level. Since OCT signal attenuation is likely to occur at depths below the RPE as well as underneath drusen, OCTA of the CC can be susceptible to such attenuation artifacts. In order to mitigate this potential source of error, when evaluating OCTA images of the CC we also evaluated the co-registered OCT intensity images to confirm that signal levels were sufficient for accurate OCTA measurements (see for example, Figure 4B, and Figure 5, row 2). Additionally, the VCSEL light source used in this study operates at a ~1050 nm wavelength, compared to commercial systems, which use light sources operating at ~840 nm. Images of the CC at ~1050 nm are less likely to be affected by ocular opacity and attenuation artifacts.[40] Finally, for OCTA images of the CC in regions of GA, OCT signal attenuation is not a concern because of RPE atrophy.

Some discussion regarding the wider applicability of the VISTA algorithm is also merited. Since VISTA is a software technique and is agnostic to the underlying hardware it can be used on both spectral domain OCT (SDOCT) systems as well as SSOCT systems. The

principal requirement of VISTA is that 3 or more repeated B-scans are acquired at each fundus position. Using ultrahigh speed OCT system we were able achieve 3 mm × 3 mm and 6 mm × 6 mm fields of view with 5 repeated B-scans. Imaging with a slower A-scan rate system, however, would require trade-offs in pixel density, imaging area, or acquisition time. In principle, VISTA could be applied to the commercial Avanti RTVue XR (Optovue) system; however, this instrument currently uses 2 repeated B-scans for OCTA in order to optimize imaging area. The Avanti system is currently configured with a ~5 ms interscan time, while the study reported here uses ~1.5 ms and ~3.0 ms interscan times. Thus, while the Avanti system has a higher flow sensitivity than our system, because of saturation effects it has a comparatively limited ability to distinguish differences in flow speeds. Furthermore, because the Avanti images at 840 nm wavelengths, it is more susceptible to attenuation artifacts, especially when imaging the CC.

In this manuscript new terminology has been introduced describing OCTA protocols (Table 1) as well as *en face* OCTA of the CC (Table 2). In particular, this study emphasizes the importance of specifying the interscan time because this parameter sets the slowest detectable flow and the fastest distinguishable flow in OCTA (Figure 1). Vasculature having slow flow can appear silent on OCTA. Conversely, different flows can be indistinguishable on OCTA because of saturation effects. The use of VISTA can improve the ability to differentiate different flows and degrees of flow impairment. It can also improve sensitivity to slow flows, up to a sensitivity limit set by parasitic eye motion. In general, we found that interpretation of OCTA of the CC requires careful examination of *en face* OCTA data in conjunction with *en face* structural OCT, cross sectional OCTA, and cross sectional structural OCT data.

A limitation of the current study is that the number of normal subjects was small and their mean age was younger than that of the patients with GA. The need to investigate an age-matched group of normal subjects is further underscored by the fact that a decrease in CC density as a function of age has been observed.[28]

In summary, although more comprehensive studies are required, we believe that OCTA is a promising modality for noninvasive imaging of retinal, CC, and choroidal vasculatures. The role of the interscan time in governing the dynamic range of OCTA is important and should be controlled in future studies. VISTA is a useful methodology for distinguishing varying degrees of CC flow impairment and promises to be important for elucidating the pathogenesis of GA in non-exudative AMD. The observation that CC flow impairment is present outside the region of GA and the ability to assess different degrees of flow impairment may provide a surrogate marker for progression as well as treatment response in future pharmaceutical trials for non-exudative AMD.

Acknowledgments

Financial Support

This work was supported by the National Institute of Health (NIH R01-EY011289-27, R44-EY022864-01, R44-EY022864-02, R01-CA075289-16), Air Force Office of Scientific Research (AFOSR FA9550-10-1-0551 and FA9550-12-1-0499), a Samsung Scholarship, and by a Natural Sciences and Engineering Research Council of Canada Scholarship.

References

1. Sarks JP, Sarks SH, Killingsworth MC. Evolution of geographic atrophy of the retinal-pigment epithelium. Eye. 1988; 2:552–77. [PubMed: 2476333]
2. McLeod DS, Grebe R, Bhutto I, et al. Relationship between RPE and choriocapillaris in age-related macular degeneration. Investigative Ophthalmology & Visual Science. 2009; 50:4982–91. [PubMed: 19357355]
3. Mullins RF, Johnson MN, Faidley EA, et al. Choriocapillaris vascular dropout related to density of drusen in human eyes with early age-related macular degeneration. Investigative Ophthalmology & Visual Science. 2011; 52:1606–12. [PubMed: 21398287]
4. Bhutto I, Lutty G. Understanding age-related macular degeneration (AMD): Relationships between the photoreceptor/retinal pigment epithelium/Bruch's membrane/choriocapillaris complex. Molecular Aspects of Medicine. 2012; 33:295–317. [PubMed: 22542780]
5. Biesemeier A, Taubitz T, Julien S, et al. Choriocapillaris breakdown precedes retinal degeneration in age-related macular degeneration. Neurobiology of Aging. 35:2562–73. [PubMed: 24925811]
6. Mullins, RF.; Khanna, A.; Schoo, DP., et al. Is age-related macular degeneration a microvascular disease?. In: Ash, JD.; Grimm, C.; Hollyfield, JG., et al., editors. Retinal Degenerative Diseases. Vol. 801. Springer; New York: 2014. p. 283-9.
7. McLeod DS, Taomoto M, Otsuji T, et al. Quantifying changes in RPE and choroidal vasculature in eyes with age-related macular degeneration. Investigative Ophthalmology & Visual Science. 2002; 43:1986–93. [PubMed: 12037009]
8. Bischoff P, Flower R. Ten years experience with choroidal angiography using indocyanine green dye: a new routine examination or an epilogue? Documenta Ophthalmologica. 1985; 60:235–91. [PubMed: 2414083]
9. Flower RW. Extraction of choriocapillaris hemodynamic data from ICG fluorescence angiograms. Investigative Ophthalmology & Visual Science. 1993; 34:2720–9. [PubMed: 8344794]
10. Zhu L, Zheng Y, von Kerczek CH, et al. Feasibility of extracting velocity distribution in choriocapillaris in human eyes from ICG dye angiograms. Journal of Biomechanical Engineering. 2005; 128:203–9. [PubMed: 16524331]
11. Makita S, Hong Y, Yamanari M, et al. Optical coherence angiography. Optics Express. 2006; 14:7821–40. [PubMed: 19529151]
12. Fingler J, Schwartz D, Yang CH, et al. Mobility and transverse flow visualization using phase variance contrast with spectral domain optical coherence tomography. Optics Express. 2007; 15:12636–53. [PubMed: 19550532]
13. Tao YK, Davis AM, Izatt JA. Single-pass volumetric bidirectional blood flow imaging spectral domain optical coherence tomography using a modified Hilbert transform. Optics Express. 2008; 16:12350–61. [PubMed: 18679512]
14. An L, Wang RKK. In vivo volumetric imaging of vascular perfusion within human retina and choroids with optical micro-angiography. Optics Express. 2008; 16:11438–52. [PubMed: 18648464]
15. Mariampillai A, Standish BA, Moriyama EH, et al. Speckle variance detection of microvasculature using swept-source optical coherence tomography. Optics Letters. 2008; 33:1530–2. [PubMed: 18594688]
16. Vakoc BJ, Lanning RM, Tyrrell JA, et al. Three-dimensional microscopy of the tumor microenvironment in vivo using optical frequency domain imaging. Nature Medicine. 2009; 15:1219–23.
17. Yu LF, Chen ZP. Doppler variance imaging for three-dimensional retina and choroid angiography. Journal of Biomedical Optics. 2010; 15:016029. [PubMed: 20210473]
18. Jonathan, E.; Enfield, J.; Leahy, MJ. Correlation mapping: rapid method for retrieving microcirculation morphology from optical coherence tomography intensity images. In: Tuchin, VV.; Duncan, DD.; Larin, KV., et al., editors. Dynamics and Fluctuations in Biomedical Photonics VIII. San Francisco, California: SPIE; 2011.
19. Blatter C, Klein T, Grajciar B, et al. Ultrahigh-speed non-invasive widefield angiography. Journal of Biomedical Optics. 2012; 17

20. Kim DY, Fingler J, Zawadzki RJ, et al. Optical imaging of the chorioretinal vasculature in the living human eye. Proceedings of the National Academy of Sciences of the United States of America. 2013; 110:14354–9. [PubMed: 23918361]
21. Schwartz DM, Fingler J, Kim DY, et al. Phase-variance optical coherence tomography: a technique for noninvasive angiography. Ophthalmology. 2014; 121:180–7. [PubMed: 24156929]
22. Grulkowski I, Liu JJ, Potsaid B, et al. Retinal, anterior segment and full eye imaging using ultrahigh speed swept source OCT with vertical-cavity surface emitting lasers. Biomedical Optics Express. 2012; 3:2733–51. [PubMed: 23162712]
23. Choi W, Potsaid B, Jayaraman V, et al. Phase-sensitive swept-source optical coherence tomography imaging of the human retina with a vertical cavity surface-emitting laser light source. Optics Letters. 2013; 38:338–40. [PubMed: 23381430]
24. Unterhuber A, Povazay B, Hermann B, et al. In vivo retinal optical coherence tomography at 1040 nm-enhanced penetration into the choroid. Optics Express. 2005; 13:3252–8. [PubMed: 19495226]
25. Guizar-Sicairos M, Thurman ST, Fienup JR. Efficient subpixel image registration algorithms. Optics Letters. 2008; 33:156–8. [PubMed: 18197224]
26. Tokayer J, Jia Y, Dhalla AH, et al. Blood flow velocity quantification using split-spectrum amplitude-decorrelation angiography with optical coherence tomography. Biomedical Optics Express. 2013; 4:1909–24. [PubMed: 24156053]
27. Makita S, Jaillon F, Yamanari M, et al. Comprehensive in vivo micro-vascular imaging of the human eye by dual-beam-scan Doppler optical coherence angiography. Optics Express. 2011; 19:1271–83. [PubMed: 21263668]
28. Ramrattan RS, van der Schaft TL, Mooy CM, et al. Morphometric analysis of Bruch's membrane, the choriocapillaris, and the choroid in aging. Investigative Ophthalmology & Visual Science. 1994; 35:2857–64. [PubMed: 8188481]
29. Flower RW, von Kerczek C, Zhu L, et al. Theoretical investigation of the role of choriocapillaris blood flow in treatment of subfoveal choroidal neovascularization associated with age-related macular degeneration. American Journal of Ophthalmology. 132:85–93. [PubMed: 11438059]
30. Moult EM, Choi W, Waheed NK, et al. Ultrahigh-speed swept-source OCT angiography in exudative AMD. Ophthalmic Surgery, Lasers and Imaging Retina. 2014; 45:496–505.
31. Olver JM. Functional anatomy of the choroidal circulation: methyl methacrylate casting of human choroid. Eye. 1990; 4:262–72. [PubMed: 2379644]
32. Choi W, Mohler KJ, Potsaid B, et al. Choriocapillaris and choroidal microvasculature imaging with ultrahigh speed OCT angiography. PLOS ONE. 2013; 8:e81499. [PubMed: 24349078]
33. Abbey A, Kuriyan A, Modi Y, et al. Optical coherence tomography measurements of choroidal thickness in healthy eyes: correlation with age and axial length. Ophthalmic Surgery, Lasers and Imaging Retina. In press.
34. Mullins R, Grassi MJS. Glycoconjugates of choroidal neovascular membranes in age-related macular degeneration. Molecular Vision. 2005; 11:509–17. [PubMed: 16052166]
35. McLeod DS, Lutty GA. High-resolution histologic analysis of the human choroidal vasculature. Investigative Ophthalmology & Visual Science. 1994; 35:3799–811. [PubMed: 7928177]
36. Bird AC, Phillips RL, Hageman GS. Geographic atrophy: a histopathological assessment. JAMA Ophthalmology. 2014; 132:338–45. [PubMed: 24626824]
37. Wolf-Schnurrbusch UEK, Enzmann V, Brinkmann CK, et al. Morphologic changes in patients with geographic atrophy assessed with a novel spectral OCT–SLO combination. Investigative Ophthalmology & Visual Science. 2008; 49:3095–9. [PubMed: 18378583]
38. Fleckenstein M, Issa PC, Helb HM, et al. High-resolution spectral domain-OCT imaging in geographic atrophy associated with age-related macular degeneration. Investigative Ophthalmology & Visual Science. 2008; 49:4137–44. [PubMed: 18487363]
39. Sunness JS, Gonzalez-Baron J, Bressler NM, et al. The development of choroidal neovascularization in eyes with the geographic atrophy form of age-related macular degeneration. Ophthalmology. 1999; 106:910–9. [PubMed: 10328389]
40. Povazay B, Hermann B, Unterhuber A, et al. Three-dimensional optical coherence tomography at 1050 nm versus 800 nm in retinal pathologies: enhanced performance and choroidal penetration in cataract patients. Journal of Biomedical Optics. 2007; 12:041211. [PubMed: 17867800]

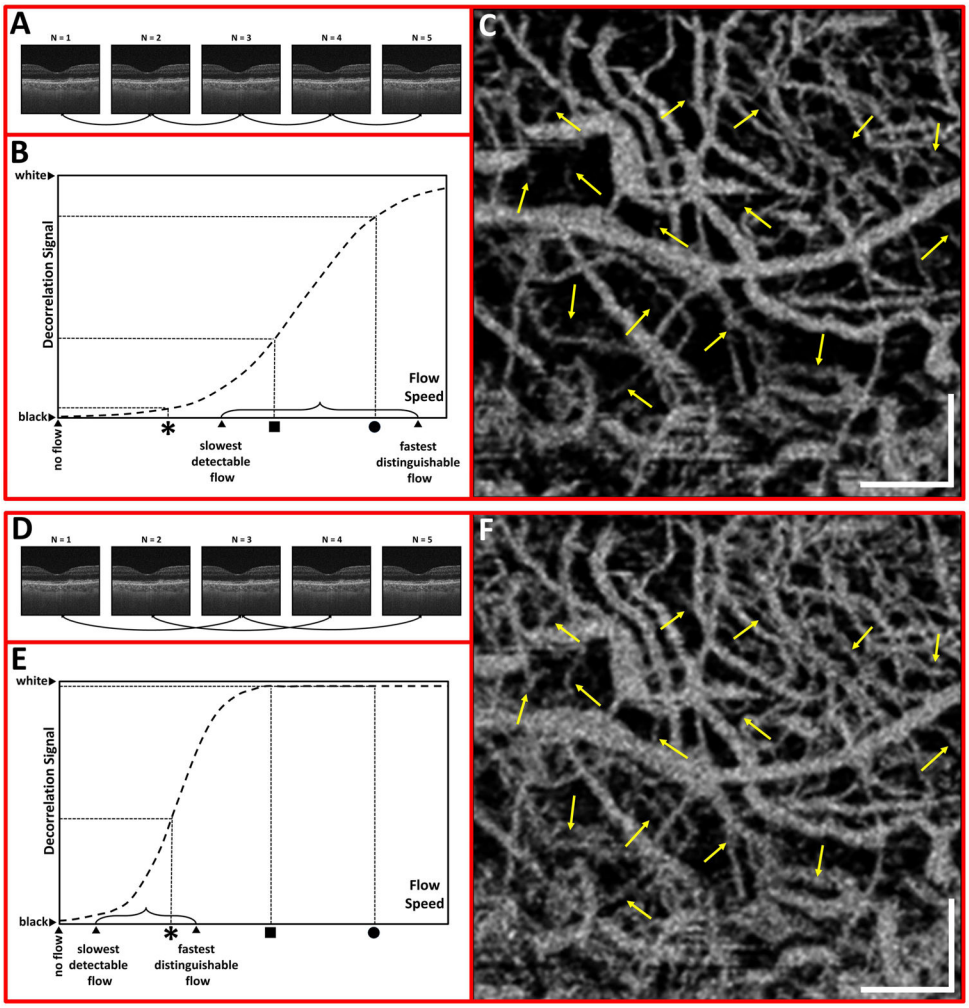

Figure 1.

Illustration of variable interscan time analysis (VISTA). Optical coherence tomography angiography (OCTA) data is generated using 5 repeated B-scans (N = 1 to 5) from the same location, as shown schematically in (A) and (D). The time between repeated B-scans (interscan time) was ~1.5 ms. It is possible to calculate the OCTA decorrelation using adjacent B-scans, as in (A), or every-second B-scan, as in (D), which doubles the interscan time to ~3.0 ms. (B) and (E) show idealized plots of the OCTA decorrelation signal versus erythrocyte flow speed. The plots are intended to represent general trends rather than exact functional form. The OCTA dynamic range, demarcated by the brackets, spans the range between the slowest detectable flow and the fastest distinguishable flow. The dynamic range both shifts and compresses as the interscan time is doubled (B) and (E). Note that the slow flow marked by the asterisk will not be detectable using the ~1.5 ms interscan time of (B) but becomes detectable using the longer ~3.0 ms interscan time of (E). The longer ~3.0 ms interscan time provides high sensitivity to slow flows. Note, however, that the faster flows marked by the square and circle are saturated (faster than the fastest distinguishable flow) using the ~3.0 ms interscan time of (E). The shorter ~1.5 ms interscan time of (B) is thus superior for the purpose of distinguishing the flows corresponding to the circle and square.

Variable interscan time analysis (VISTA) is required because a fixed interscan time cannot simultaneously visualize and distinguish the flows marked the asterisk, the square, and the circle. (C) and (F) show *en face* OCTA images of choroidal vessels in a region of GA. The scale bars are 500 μm and the images are enlarged views from a 6 mm × 6 mm field of view. (C) is obtained using a ~1.5 ms interscan time, whereas (F) is obtained using a ~3.0 ms interscan time. To facilitate comparison, arrows are superimposed on the two images. Note many vessels that are visible in (F) are only partially visible or completely absent in (C).

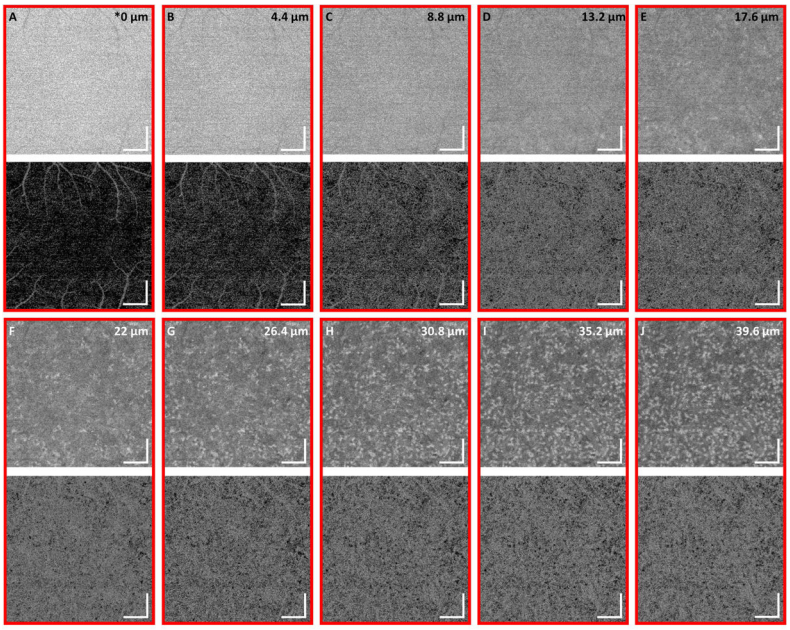

Figure 2.

Depth dependence of *en face* optical coherence tomography (OCT) and optical coherence tomography angiography (OCTA). All images are from a 35-year-old normal subject. For (A–J) the top image is a 4.4 µm *en face* OCT slab and the bottom image is a 4.4 µm *en face* OCTA slab. Starting at (A), to which we arbitrarily assign the reference depth of 0 µm to a slab laying within the RPE, each of (A–J) is separated by 4.4 µm from its neighboring slabs; (A–J) are at progressively deeper positions in the OCT and OCTA volumes. For example, (B) shows the 4.4 µm *en face* OCT and OCTA slabs 4.4 µm below (A), and (J) shows the 4.4 µm *en face* OCT and OCTA slabs 39.6 µm below (A). The slabs in (A) are located above the choriocapillaris (CC) and correspond to tissue without flow; the vessels seen in (A) are an artifact of OCTA decorrelation tails from the overlying retinal vasculature. The CC corresponds, approximately, to the slabs of (C) and (D). Note that the CC is not visible in the OCT slabs. The CC produces OCTA decorrelation tails onto the underlying slabs (E–J), the patterning of which is persistent in depth and still present in (J). The depth persistence caused by the OCTA decorrelation tails allows the patterning of the CC vasculature to be inferred by examining the slabs underlying the CC. All scale bars are 500 µm.

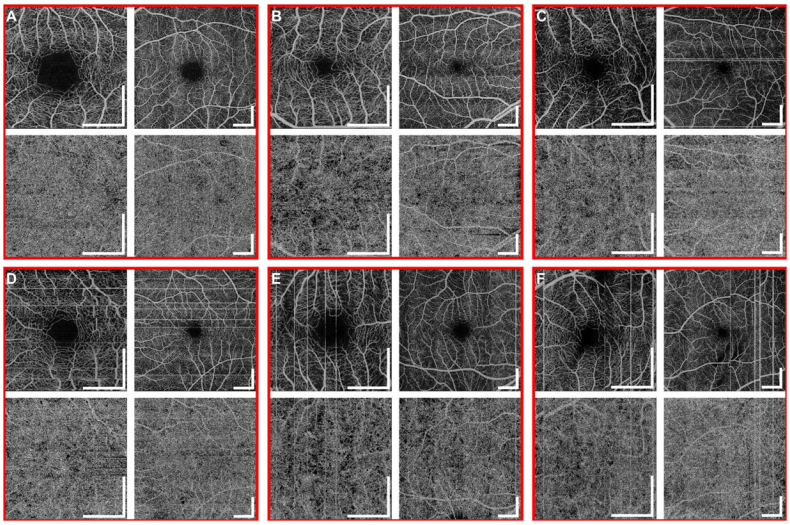

Figure 3.

En face optical coherence tomography angiography (OCTA) of the retinal and choriocapillaris (CC) vasculatures from (A) 35, (B) 53, (C) 58, (D) 68, (E) 65, and (F) 70-year-old normal subjects. For each subject (A–F), the top left and top right images are mean *en face* projections of the OCTA volume through the depths spanned by the retinal vasculature, over 3 mm × 3 mm and 6 mm × 6 mm fields of view, respectively; the bottom left and bottom right images are 4.4 μm thick *en face* OCTA CC slabs of 3 mm × 3 mm and 6 mm × 6 mm fields of view, respectively. The term *CC slab* refers to a slab of the OCTA volume that lies below the actual CC, but that reflects the CC patterning, and therefore CC flow. In normal eyes, the CC vessel ratio was generally high and the CC decorrelation signal was relatively dense and homogeneous. Note that retinal vessels produce OCTA decorrelation tails in the *en face* OCTA CC slabs. The straight vertical and horizontal white lines are eye motion artifacts; their direction depends on the orientation of the OCT fast scan axis during acquisition. All scale bars are 1 mm.

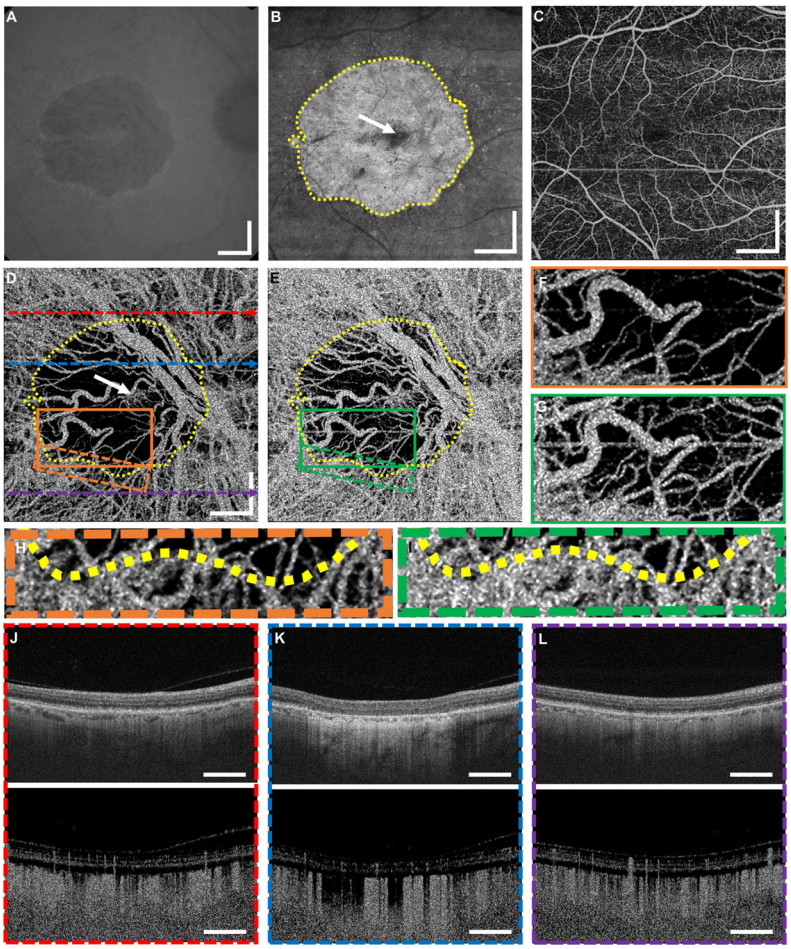

Figure 4.

Fundus autofluorescence (FAF), optical coherence tomography (OCT) and optical coherence tomography angiography (OCTA) in a 75-year-old patient with non-exudative age-related macular degeneration (AMD) with geographic atrophy (GA). This patient had a visual acuity of 20/20. The FAF (A) and the mean *en face* projection of the entire OCT volume (B) clearly show the region of GA, outlined by the yellow dashed contour in (B). The GA region appears lighter due to increased light penetration into the choroid caused by RPE atrophy. The white arrow indicates the region of foveal sparing. (C) shows a mean *en face* projection of the OCTA volume through the depths spanned by the retinal vasculature. The retinal vasculature appears normal. (D) shows a 4.4 μm thick *en face* OCTA choriocapillaris (CC) slab corresponding to a ~1.5 ms interscan time. The yellow dashed contour from (B) is superimposed, and pronounced CC alteration appears within it. CC flow in the area of foveal sparing, indicated by the white arrow, is also visible. CC alteration is also evident outside the GA margin. (E) shows the same 4.4 μm thick *en face* OCTA choriocapillaris (CC) slab as in (D), but corresponding to a ~3.0 ms interscan time. Note how some areas with low decorrelation signal in (D) have increased decorrelation signal in (E), suggesting flow impairment, not atrophy. Enlarged views of the solid orange and green boxes of (D) and (E) are shown in (F) and (G), respectively. Note that some choroidal vessels that are not visible in (F) become visible in (G). Enlarged views of the dashed orange

and green boxes of (D) and (E) are shown in (H) and (I), respectively. Note that some of the regions with low decorrelation signal in (H) have a higher decorrelation signal in (I), suggesting flow impairment along the GA margin. OCT (top) and OCTA (bottom) B-scans through the red, blue, and purple horizontal dashed lines in (D) are shown in (J), (K), and (L), respectively. All scale bars are 1 mm.

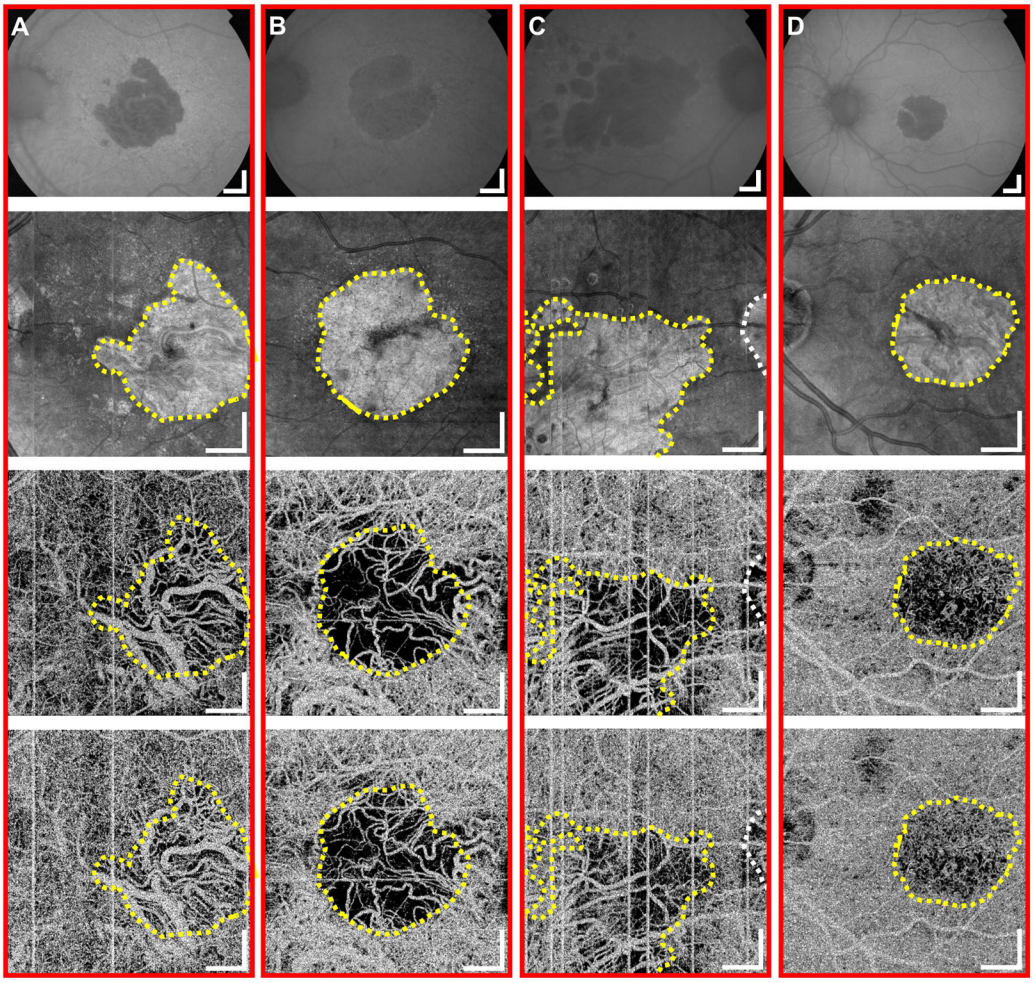

Figure 5.

Optical coherence tomography (OCT) and optical coherence tomography angiography (OCTA) of (A) 78, (B) 76, (C) 82, and (D) 71-year-old patients, respectively, all with non-exudative age-related macular degeneration (AMD) with geographic atrophy (GA). For each patient (A–D), the top image is the fundus autofluorescence (FAF) and the second-to-top image is the mean *en face* projection of the entire OCT volume. The region of GA is outlined by a yellow dashed contour; peripapillary atrophy is outlined by a white dashed contour. For each patient (A–D), 4.4 μm thick *en face* OCTA choriocapillaris (CC) slabs are shown in the second-to-bottom and bottom images. The second-to-bottom images correspond to a ~1.5 ms interscan time and the bottom images correspond to a ~3.0 ms interscan time. The *en face* OCTA CC slabs of (A–C) show flow impairment adjacent to the GA margin while that of (D) shows normal flow adjacent to the GA margin. All scale bars are 1 mm.

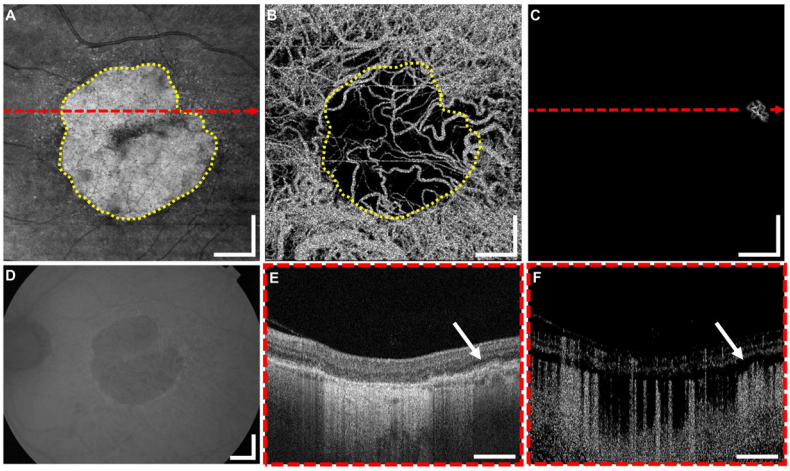

Figure 6.

An example of clinically undetected choroidal neovascularization (CNV) in a 75-year-old patient with age-related macular degeneration (AMD) with geographic atrophy (GA). The mean *en face* projection of the entire OCT volume (A) clearly shows the region of GA, outlined by the yellow dashed contour. The GA region appears lighter due to increased light penetration into the choroid caused by RPE atrophy. (B) shows a 4.4 μm thick *en face* OCTA choriocapillaris (CC) slab corresponding to a ~1.5 ms interscan time. The yellow dashed contour from (A) is superimposed and pronounced CC alteration appears inside and outside of this contour. (C) shows a mean *en face* projection of the OCTA volume through the depths spanned by the CNV. OCTA shadowing artifacts from retinal vasculature have been manually removed to improve clarity. (D) shows a fundus autofluorescence (FAF) of the region of GA. The OCT and OCTA B-scans, extracted from the red dashed lines in (A) and (C) are shown in (E) and (F), respectively. The white arrows in (E) and (F) indicate the CNV lesion. Note that the lesion is located above surviving RPE cells. All scale bars are 1 mm.

Table 1

General terminology for describing OCTA acquisition.

Decorrelation signal: a quantitative surrogate for blood flow. The decorrelation signal is calculated on a pixel-by-pixel basis by comparing two B-scans acquired at the same position at two different times (separated by the interscan time). The decorrelation signal increases with increasing blood flow, but has a limited dynamic range. There is a slowest detectable flow and a fastest distinguishable flow. An OCTA image is generated by displaying the decorrelation signal as a grayscale image. In this manuscript we use the convention of associating lighter shaded pixels with larger decorrelations and darker shaded pixels with smaller decorrelations.
Slowest detectable flow: the slowest flow that produces a detectable decorrelation signal. Flows that are slower than the slowest detectable flow produce decorrelation signals that are indistinguishable from background noise and are thus undetectable; such flows do not appear on OCTA images.
Fastest distinguishable flow: the fastest flow such that the decorrelation signal is not saturated. Flows that are faster than the fastest distinguishable flow all produce similar decorrelation signals and are therefore indistinguishable from one another; such flows appear white on OCTA images.
Interscan time: the time between repeated B-scans. Increasing the interscan time increases the decorrelation signal, reducing both the slowest detectable flow and the fastest distinguishable flow. Thus, increasing the interscan time makes OCTA more sensitive to slower flows, but makes faster flows harder to distinguish. Decreasing the interscan time has the inverse effect.

Table 2

Terminology for describing *en face* OCTA of the CC.

Choriocapillaris alteration: any alteration in an *en face* OCTA CC slab. CC alteration can be caused by either flow impairment or atrophy.
Choriocapillaris flow impairment: reduced blood flow as manifested by a low or absent decorrelation signal. Flow impaired regions may exhibit an increased decorrelation signal if the interscan time is increased. In particular, using VISTA to shift the slowest detectable flow, the flow speed in a region of choriocapillaris flow impairment may move from being below the slowest detectable flow to being above the slowest detectable flow; this change will manifest as an increase in the decorrelation signal. If, however, the flow speed in a region of choriocapillaris flow impairment remains below the slowest detectable flow, even after the increase in interscan time, the decorrelation signal will not increase.
Choriocapillaris atrophy: decay or loss of choriocapillaris vasculature. Atrophy, like flow impairment, manifests as a low or absent decorrelation signal. However, increasing the interscan time does not increase the decorrelation signal in an atrophic region because there is no flow. This definition of atrophy includes non-perfused vessels, or “ghost vessels,” which retain their basement membrane despite losing their endothelium.
Choriocapillaris vessel ratio: for a given *en face* OCTA CC slab, the vessel ratio is defined as the total area having flows faster than the slowest detectable flow, divided by the total area having flows slower than the slowest detectable flow. Since the vessel ratio depends on the slowest detectable flow, the interscan time must be specified; increasing the interscan time will increase the vessel ratio because slower flows will be detected.

Table 3

Subject characteristics.

	Subjects imaged	Eyes imaged	Age ± std. (years)	Sex (males; females)	Race (African; Asian; Caucasian)
Normal subjects	32	63	40.7 ± 14.1	13; 19	3; 4; 25
Patients with non- exudative AMD with GA	7	12	75.9 ± 6.1	6; 1	0; 0; 7
Total	39	75			